nature climate change

LETTERS

https://doi.org/10.1038/s41558-019-0512-y

Widespread increase of boreal summer dry season length over the Congo rainforest

Yan Jiang[1], Liming Zhou[1*], Compton J. Tucker[2], Ajay Raghavendra[1], Wenjian Hua[1,3], Yi Y. Liu[4] and Joanna Joiner[2]

Dry season length strongly influences tropical rainforest vegetation and is largely determined by precipitation patterns[1,2]. Over the Amazon, the dry season length has increased since 1979 and severe short-term droughts have occurred[3,4]. However, similar changes have not been investigated for the world's second largest rainforest, the Congo Basin, where long-term drying and large-scale declines in forest greenness and canopy water content were reported[5]. Here we present observational evidence for widespread increases in the boreal summer (June–August) dry season length over the Congo Basin since the 1980s, from both hydrological and ecological perspectives. We analysed both dry season onset and dry season end via multiple independent precipitation and satellite-derived vegetation datasets for the period 1979–2015. The dry season length increased by 6.4–10.4 days per decade in the period 1988–2013, primarily attributed to an earlier dry season onset and a delayed dry season end. The earlier dry season onset was caused by long-term droughts due to decreased rainfall in the pre-dry season (April–June). The delayed dry season end resulted from insufficiently replenished soil moisture, which postpones the start of the next wet season and hinders vegetation regrowth. If such changes continue, the enhanced water stress in a warming climate may affect the carbon cycle and alter the composition and structure of evergreen rainforest[1,6].

One distinct feature of tropical rainforests is the seasonal transition between dry and wet seasons. In the tropics, dry seasons represent periods with low rainfall and coincide with the seasonal shift of the rain belt over the course of the year[7]. Tropical rainforests are often considered as light-limited rather than water-limited due to persistent cloudiness and adequate water availability[8]. Previous studies based on in situ and satellite observations over the Amazon suggested that peak photosynthesis coincides with peak irradiance over humid rainforest in the dry season[8,9]. Photosynthesis continues because the deep roots of trees can access groundwater, allowing them to grow during the sunnier and drier part of the year[9]. However, soil moisture becomes a limiting factor due to enhanced evapotranspiration and low rainfall as the dry season progresses, making tropical rainforests water-limited rather than light-limited[10]. Any large change in rainfall seasonality that modifies the dry season length (DSL) and intensity, rainfall amount and insolation availability may influence the photosynthesis and productivity of a tropical rainforest.

Dry season duration is closely related to the frequency of droughts and affects the composition of local vegetation. Short-term droughts have immediate impacts on vegetation greenness. Three major droughts, in 2005, 2010 and 2016, occurred in the Amazon, causing decreases in the water level of the Amazon River and in forest photosynthetic capacity[11–13]. A more intense and longer dry season will enhance the frequency and intensity of short-term droughts and eventually alter the distribution and structure of forest vegetation[6].

The Congo Basin has experienced a long-term drying trend. Consequently, forest browning, reduced canopy water content and decreased rainfall have been detected by multiple satellites in recent decades[5,14]. However, changes in dry season duration have never been studied and are poorly understood over the Congolese rainforest. Unlike the Amazon, the Congo has a drier climate with less annual rainfall, more fragmented forest surrounded by tropical savannas with high fire counts and a higher percentage of semi-deciduous vegetation. Therefore, the Congo rainforest is thus more sensitive and less resilient to climate changes[15]. The Congolese rainforest might be tolerant to short-term rainfall reduction, but long-term drying may result in transition from higher-biomass and closed-canopy forests to lower-biomass and open-canopy forests[5]. Hence, variations in the DSL over the Congo have important ecological, societal and climate implications. Furthermore, previous studies on DSL changes in the Amazon were based on analysis from the hydrological perspective only, while little attention was paid to the ecological perspective[3]. Here we analysed DSL changes over the Congo Basin from both hydrological and ecological perspectives.

One difficulty in studying DSL variations over the Congo is the complicated seasonality of precipitation. The seasonality varies with distance to the equator and along a west-to-east gradient. A zonal strip (4° N–4 °S) extending over equatorial Africa is identified as a region of bimodal precipitation (Supplementary Fig. 1a). Peak rainfall in the bimodal region occurs during transitional seasons, corresponding to the northward and southward passages of the rain belt (Supplementary Fig. 1b–e). Our study focuses on the Congo Basin (12° E–32° E, 5° N–6° S) during the June–August (JJA) dry season given the long-term drying trend observed in equatorial Africa during the pre-dry season (April–June, AMJ)[14], which is expected to affect the following dry season. The study domain is carefully chosen to cover the contiguous forested area with similar precipitation patterns and limited anthropogenic and orographic influences (Supplementary Figs. 1f,g and 2).

[1]Department of Atmospheric and Environmental Sciences, University at Albany, State University of New York, Albany, NY, USA. [2]NASA Goddard Space Flight Center, Greenbelt, MD, USA. [3]Key Laboratory of Meteorological Disaster, Ministry of Education, Nanjing University of Information Science & Technology, Nanjing, China. [4]School of Geographic Sciences, Nanjing University of Information Science & Technology, Nanjing, China.
*e-mail: lzhou@albany.edu

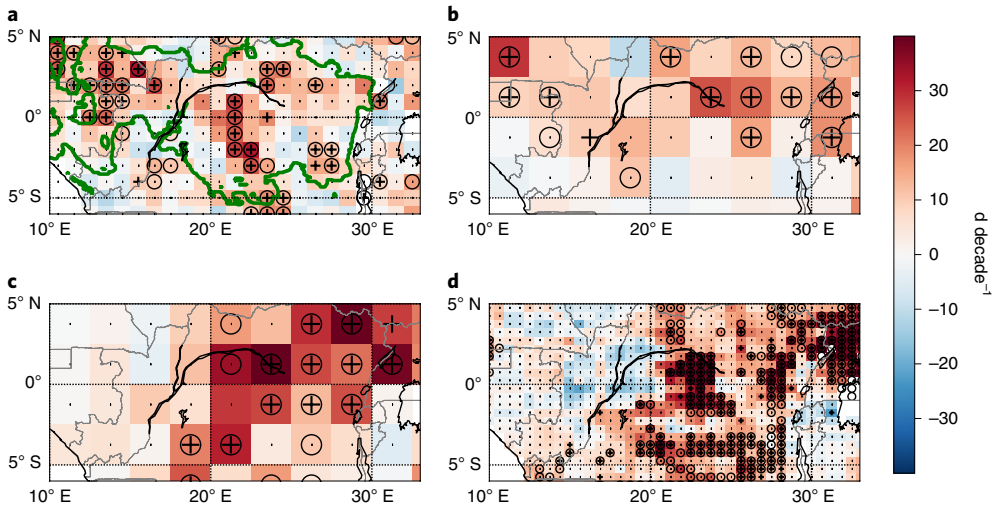

Fig. 1 | Spatial patterns of linear trends of the JJA DSL from four precipitation datasets for the period 1988–2013. a, GPCC. **b**, GPCP. **c**, CMAP. **d**, MERRA-2. The green line delineates the boundary of the Congolese rainforest. Grid boxes with crosses have a significant linear trend at $P < 0.1$. Grid boxes with circles pass the Mann–Kendall (MK) trend test and have increasing trends at the 10% significance level.

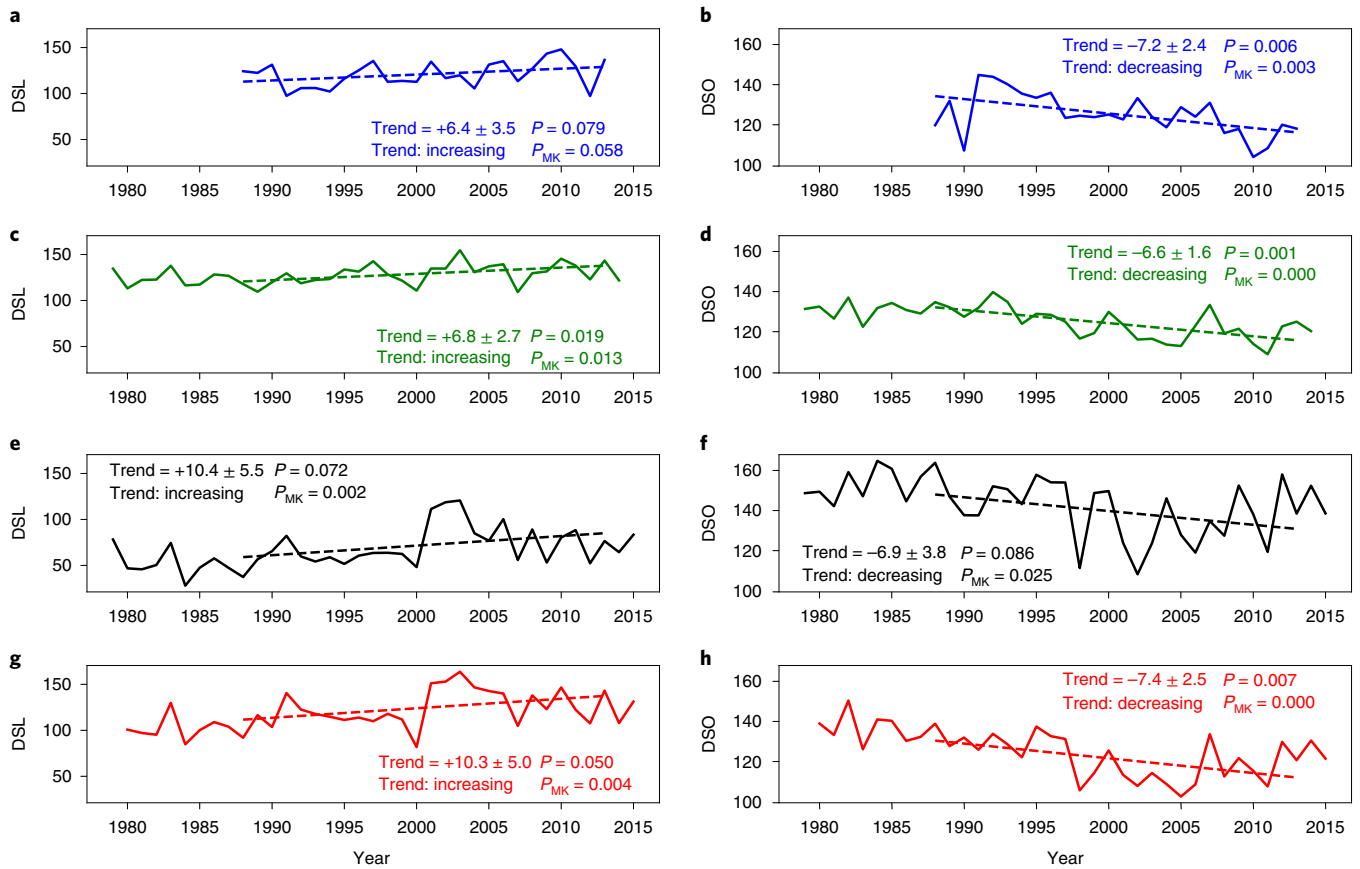

Fig. 2 | Regionally aggregated interannual variations and linear trends of the JJA DSL and DSO. a,**b**, GPCC (1988–2013). **c**,**d**, GPCP (1979–2014). **e**,**f**, CMAP (1979–2015). **g**,**h**, MERRA-2 (1980–2015). The linear trend (d decade^{-1}) and its significance level P for the period 1988–2013 are shown. Results and significance levels of the MK trend test over the full temporal span of each precipitation dataset are also included. Solid lines, interannual variations; dashed lines, linear trends.

To quantify variations in the DSL, first, the dry season onset (DSO) and dry season end DSE) for each grid box within the study region were determined using an objective method by calculation of the cumulative rainfall anomaly (see Methods and Supplementary Fig. 3). Next, trend analyses of annual DSL time series were conducted (see Methods). To overcome the paucity of observations over the Congo Basin, various precipitation data and satellite-retrieved geophysical variables were used to quantify robust DSL

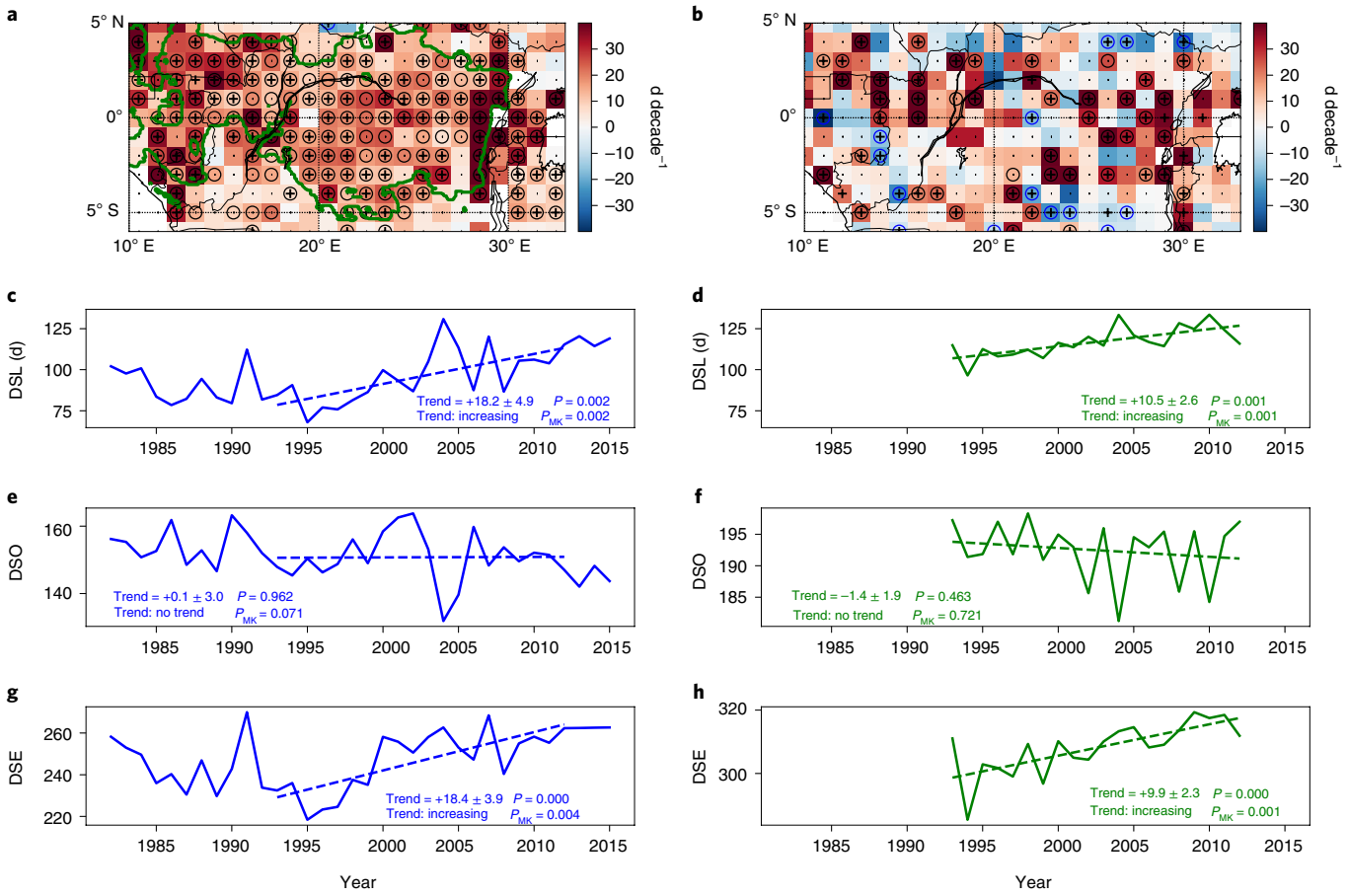

Fig. 3 | JJA dry season changes estimated by NDVI and VOD. a,**b**, Spatial patterns of linear trends of the DSL from NDVI (**a**) and VOD (**b**) for the period 1993–2012. The green line delineates the boundary of the Congolese rainforest. Grid boxes with crosses have significant linear trends ($P < 0.1$ using least squares regression), and grid boxes with circles pass the MK trend test at the 10% significance level. **c**,**d**, Regionally aggregated interannual variations (solid lines) and linear trends (dashed lines) of the DSL from NDVI (**c**) and VOD (**d**) over the Congo Basin. **e**,**f**, Same as **c**,**d**, but for the DSO. **g**,**h**, Same as **c**,**d**, but for the DSE. The linear trend (d decade^{-1}) and its significance level P for the period 1993–2012 are shown. Results and significance level of the MK trend test over the full temporal span of each dataset are also included.

changes. For the hydrological analysis, we used precipitation data from the Global Precipitation Climatology Center (GPCC)[16], Global Precipitation Climatology Project (GPCP)[17], Climate Prediction Center (CPC) Merged Analysis of Precipitation (CMAP)[18] and Modern-Era Retrospective Analysis for Research and Applications, v.2 (MERRA-2)[19]. For the ecological analysis, the preprocessed normalized difference vegetation index (NDVI)[20], newly merged vegetation optical depth (VOD)[21] passive microwave data and solar-induced fluorescence (SIF)[22] measurements using moderate-spectral resolution radiances (see Methods) were employed. NDVI represents vegetation photosynthetic capacity and correlates well with leaf area index and primary productivity[20]. VOD represents water content in above-ground woody and leaf biomass and is sensitive to long-term climate change[21]. SIF can provide a proxy for the functioning of plant photosynthesis[22].

The spatial patterns of DSL trends derived from GPCC, GPCP, CMAP and MERRA-2 are shown in Fig. 1. Although differing in spatial resolution and data sources, all rainfall datasets show a lengthening DSL ($P \lesssim 0.1$) over the Congo Basin, particularly over the central and south basin and part of the north basin, which is usually wet during JJA. GPCC and GPCP detected a longer DSL in the northwest basin as well, while CMAP and MERRA-2 showed stronger drying in the east. Overall we observed a strong drying trend over the Congo Basin, where all gridded precipitation datasets show a maximum DSL increasing rate of 30 d decade^{-1}.

Figure 2 shows the interannual variations in DSL spatially averaged over the Congo Basin from the four precipitation datasets. The DSL increased significantly, by 6.4–10.4 d decade^{-1} for the period 1988–2013, with a rapid increase around the early 2000s matching previous records of droughts in Central Africa[23]. This increased DSL is attributed to an earlier DSO, by 6.6–7.4 d decade^{-1}, with an insignificant delay in the DSE (not shown). The advanced DSO is consistent with the observed long-term decline in rainfall during AMJ.

Since rainforest is largely determined by precipitation patterns, the satellite-derived vegetation variables NDVI, VOD and SIF were utilized to provide ecological verifications for the above results. Seasonal cycles of rainfall, NDVI, VOD and SIF show that peak geophysical vegetation values lag behind peak rainfall. Vegetation variables are significantly correlated with rainfall in earlier months: NDVI lags behind rainfall by about one month ($R = 0.86$, $P = 0.000$), VOD lags by two months ($R = 0.84$, $P = 0.000$) and SIF lags by half a month ($R = 0.89$, $P = 0.000$) (Supplementary Fig. 4). Vegetation variables may detect different DSO or DSE dates due to the lagged correlations with precipitation, but the seasonal cycle in vegetation is comparable to the bimodal precipitation cycle observed over the Congo.

Figure 3 shows changes in DSL according to NDVI and VOD. DSL increased by 10.5–18.2 d decade^{-1} for the period 1993–2012, particularly over the east and west basin, while NDVI detected a significant increase in DSL in the central basin as well. There are a few grid boxes showing decreasing DSL near the edges of the rainforest

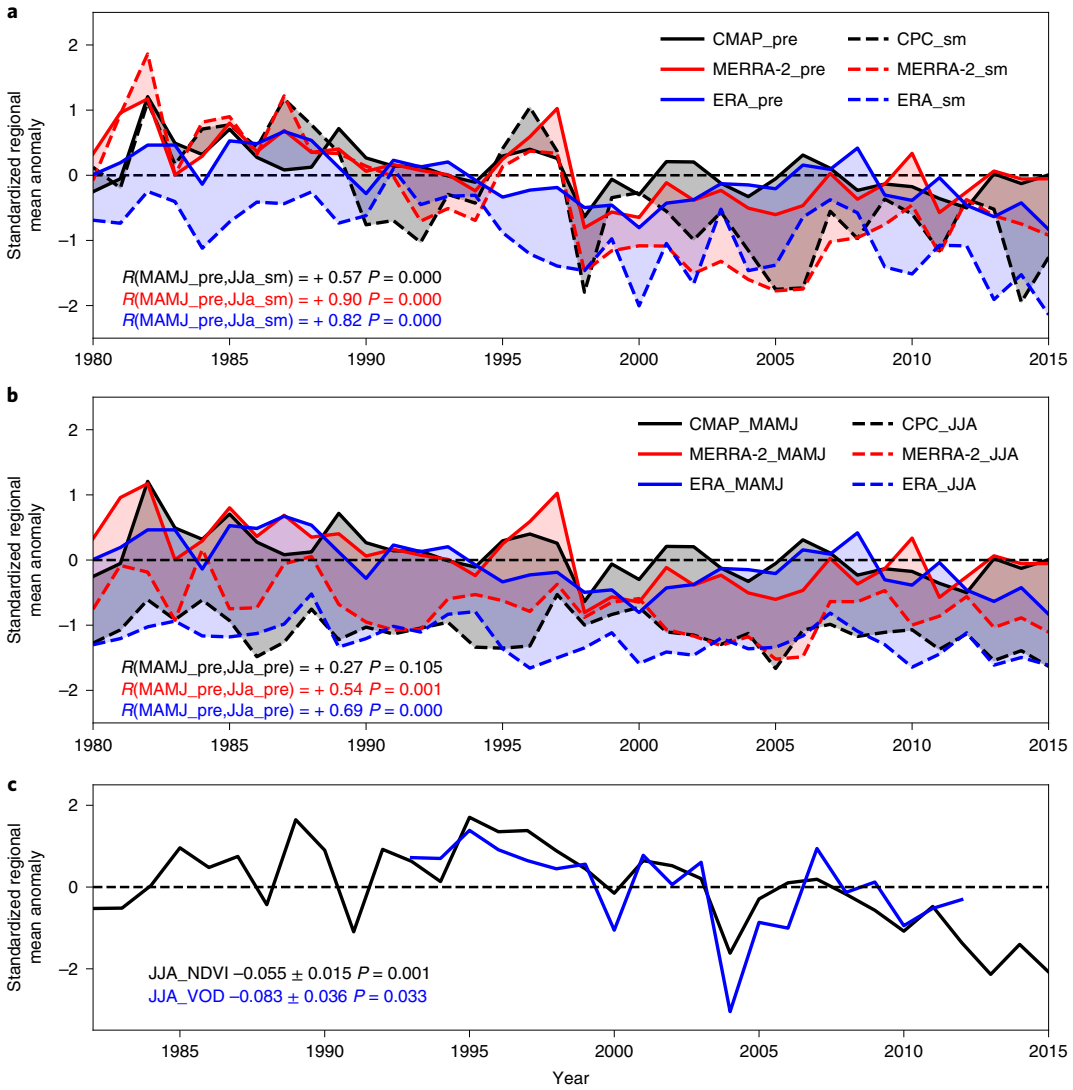

Fig. 4 | Interannual variability of standardized regional mean precipitation, soil moisture and vegetation parameters for the period 1980–2015. a, Soil moisture anomaly (dashed line) in JJA and its relationship with rainfall anomaly (solid line) during March–June (MAMJ) according to CPC, MERRA-2 and ERA-Interim. The lagged correlation *R* between soil moisture and rainfall and its significance level *P* are shown. **b**, Rainfall anomaly in JJA and its relationship with rainfall anomaly during March–June according to the CPC, MERRA-2 and ERA-Interim reanalysis datasets. The autocorrelation *R* and its significance level *P* are shown. **c**, Vegetation anomalies in JJA. Trends and significance level *P* are included. pre, precipitation; sm, soil moisture.

according to the VOD data. This is probably due to the uncertainty attributable to drought-tolerant shrublands constituting a varying mixture of grass and woody components with high water content, which may have resulted in relatively high VOD values leading to shorter DSL[21].

The lengthened DSL can mainly be attributed to a delayed DSE, which is delayed by 9.9–18.4 d decade^{-1}, indicating a delayed start of the next growing season. Differences in the spatial patterns of DSL trends among precipitation and vegetation variables are expected. Besides uncertainties in rainfall datasets, the complex lagged correlation among rainfall, soil moisture and vegetation (Fig. 4 and Supplementary Fig. 4), differences in drought tolerance among plant species and forest fragmentation also contribute to the differences[1,5]. Dense forest with deep roots has access to groundwater, delaying the inception of moisture stress through redistribution of soil moisture. Open forest with semi-deciduous vegetation has less resilience to drought and is thus more sensitive to hydrological disturbances[5,15].

The delayed DSE detected by vegetation variables coincides with the earlier DSO detected by precipitation. Higher rainfall in the months preceding the dry season replenishes groundwater, providing a water source that plants can access using deep root systems during the drier months. Therefore, the decline in precipitation during AMJ would reduce soil moisture, resulting in water stress and affecting soil rehydration and vegetation growth in the next wet season[24].

Root zone soil moisture data from CPC, MERRA-2 and ERA-Interim were analysed (see Methods). Figure 4 shows the correlation between soil moisture and rainfall. Soil moisture significantly lags behind rainfall in the precedent wet season, while autocorrelation within rainfall anomalies is much smaller and insignificant (Fig. 4b). Precipitation and soil moisture have both decreased since the 1980s: precipitation declined dramatically from March to June, by 0.24–0.42 mm d^{-1} decade^{-1} ($P = 0.001$) (Fig. 4a). Consequently, soil moisture decreased dramatically and was not fully replenished during JJA. Vegetation variables declined

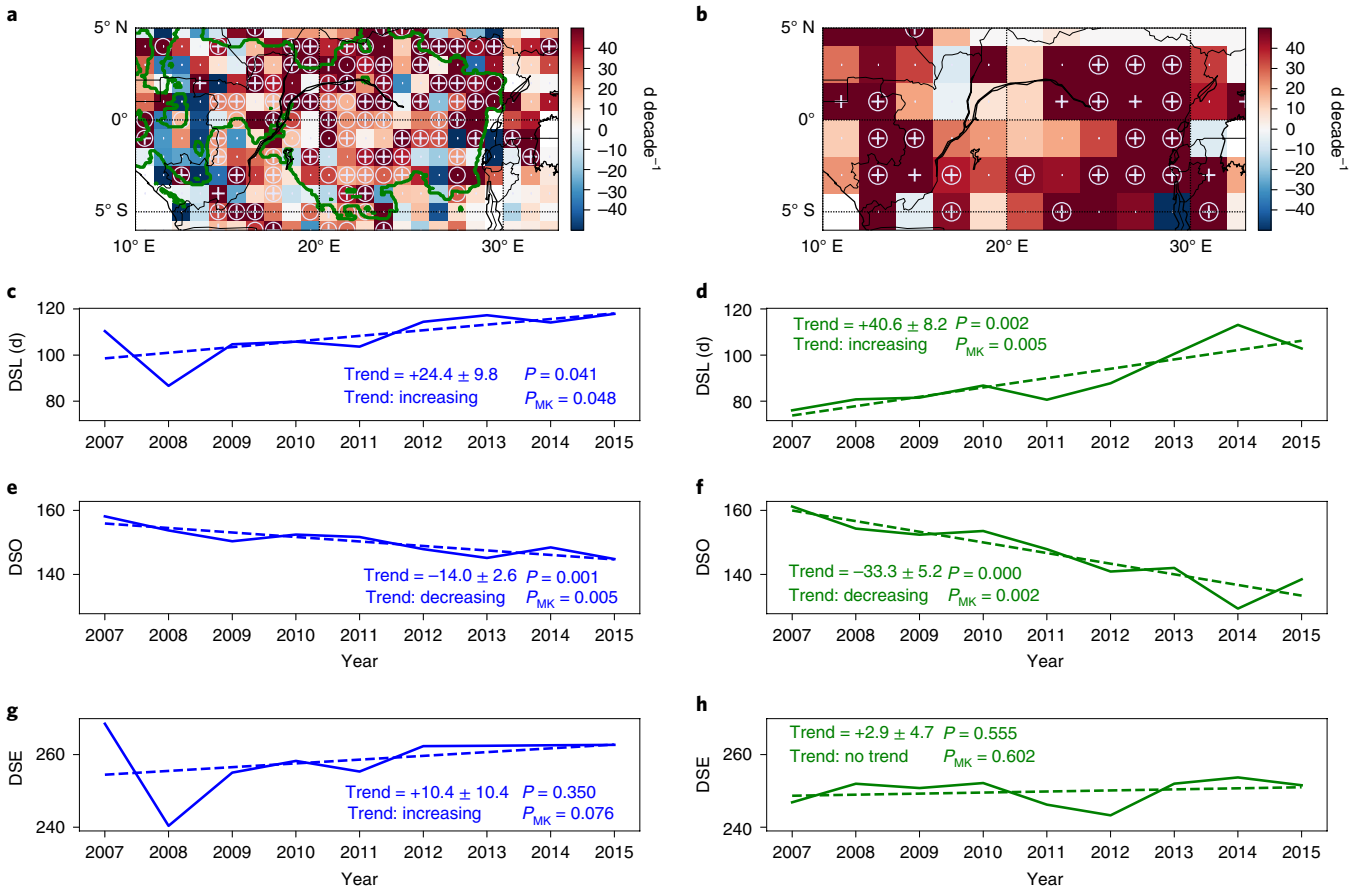

Fig. 5 | JJA dry season changes estimated by NDVI and SIF for the period 2007–2015. a,**b**, Spatial patterns of linear trends of the DSL from NDVI (**a**) and SIF (**b**). The green line delineates the boundary of the Congolese rainforest. Grid boxes with crosses have significant linear trends ($P < 0.1$ using least squares regression), and grid boxes with circles pass the MK trend test at the 10% significance level. **c**,**d**, Regionally aggregated interannual variations and linear trends of the DSL from NDVI (**c**) and SIF (**d**). **e**,**f**, Same as **c**,**d**, but for the DSO. **g**,**h**, Same as **c**,**d**, but for the DSE. The linear trend (d decade^{-1}) and its significance level P are shown. Results and significance level of the MK trend test are included.

during JJA, presumably due to the water deficit (Fig. 4c). Thus, more rainfall was required to replenish soil water deficit to stimulate rainforest growth in the next wet season (September–November). Water stress in the pedosphere elucidates how reduced precipitation at the DSO affects the vegetation phenology and leads to a delayed ecological DSE. Besides water availability, rainforests are also affected by light. However, increased photosynthetically active radiation may actually enhance water stress and adversely influence plant growth, by exacerbating water deficits during long-term droughts and longer DSL[5]. This is demonstrated by the observed delay in DSE and decline in vegetation greenness (Figs. 3g,h and 4c).

We analysed the newly developed SIF data and compared the results to NDVI data for the period 2007–2015 given the exacerbated drying trend since the 2000s (Fig. 5). DSL increased steadily and rapidly over the north, south and east Congo Basin in the latest decade, by 24.4–40.6 d decade^{-1}. The sharply increased DSL is attributed to an earlier DSO rather than to a delayed DSE, as detected by the long-term datasets over different periods. The earlier DSO can be explained by seasonal variations in precipitation and soil moisture. Soil moisture has declined during JJA since the 1980s, resulting in a water deficit during August–September at the DSE. However, the DSE water deficit reduced and recovered by approximately 2005, probably attributable to a recent increase in precipitation and soil moisture during August–September, while the decline in rainfall continued during AMJ (Supplementary Fig. 5). This shifts the water deficit to April–May, resulting in an earlier DSO driving the increase in DSL for the period 2007–2015.

Attributing the DSL variations is an important question and warrants a better understanding of precipitation over Central Africa, which is influenced by moisture transport, circulations, local evapotranspiration and orography. During the DSO, the AMJ rain belt shrank and weakened during the dry period (2000–2014) (Supplementary Fig. 5c), and this coincided with less moisture transported from the Indian Ocean due to abnormal subsidence over Central Africa and the intensification and eastward extension of the Walker circulation over the Indo-Pacific Ocean[14]. In addition, the Congo Basin is characterized by a large recycling ratio (~25%)[25]. Evapotranspiration provides considerable moisture, and land–atmosphere interactions play an important role during the dry season, particularly at the DSE, since moisture fluxes from the oceans are much weaker in August–October than in AMJ (Supplementary Fig. 6). Quantifying the contributions of different processes to the lengthened DSL should be the focus of future work.

Our research highlights an important scientific issue of dry season changes over the Congolese rainforest and their association with precipitation, vegetation and water availability under global warming. Historical records and climate models indicate increased aridity since the 1950s over Central Africa[4]. Our results show that the JJA dry season has lengthened over the Congolese rainforest since the 1980s. Consequently, the longer DSL has increased land evaporative demand, reduced cloud cover and increased surface incoming

solar radiation, which in turn amplified the aridity[26]. In addition, the Congo Basin stores extensive above-ground and underground carbon[1,27]. The local intact rainforest has become increasingly fragmented since 2001 (ref. [28]), and widespread above-ground carbon loss has been observed during the latest decade in the central and north basin[29], coinciding with the notable increasing DSL trends reported in this study. If long-term drought continues, the carbon sink is unlikely to continue but may transform to a carbon source and thus accelerate global warming[30]. This underscores the importance of studying lengthened DSL over tropical rainforests.

Online content

Any methods, additional references, Nature Research reporting summaries, source data, statements of code and data availability and associated accession codes are available at https://doi.org/10.1038/s41558-019-0512-y.

Received: 5 April 2018; Accepted: 21 May 2019;

References

1. Lewis, S. L. Tropical forests and the changing earth system. *Philos. Trans. R. Soc. Lond. B* **361**, 195–210 (2006).
2. Engelbrecht, B. M. et al. Drought sensitivity shapes species distribution patterns in tropical forests. *Nature* **447**, 80–82 (2007).
3. Fu, R. et al. Increased dry-season length over southern Amazonia in recent decades and its implication for future climate projection. *Proc. Natl Acad. Sci. USA* **110**, 18110–18115 (2013).
4. Dai, A. Increasing drought under global warming in observations and models. *Nat. Clim. Chang.* **3**, 52–58 (2013).
5. Zhou, L. et al. Widespread decline of Congo rainforest greenness in the past decade. *Nature* **509**, 86–90 (2014).
6. Fauset, S. et al. Drought-induced shifts in the floristic and functional composition of tropical forests in Ghana. *Ecol. Lett.* **15**, 1120–1129 (2012).
7. Nicholson, S. E. The ITCZ and the seasonal cycle over equatorial Africa. *Bull. Am. Meteorol. Soc.* **99**, 337–348 (2018).
8. Wright, S. J. & Van Schaik, C. P. Light and the phenology of tropical trees. *Am. Nat.* **143**, 192–199 (1994).
9. Huete, A. R. et al. Amazon rainforests green-up with sunlight in dry season. *Geophys. Res. Lett.* **33**, L06405 (2006).
10. Guan, K. et al. Photosynthetic seasonality of global tropical forests constrained by hydroclimate. *Nat. Geosci.* **8**, 284 (2015).
11. Marengo, J. A. et al. The drought of Amazonia in 2005. *J. Clim.* **21**, 495–516 (2008).
12. Marengo, J. A., Tomasella, J., Alves, L. M., Soares, W. R. & Rodriguez, D. A. The drought of 2010 in the context of historical droughts in the Amazon region. *Geophys. Res. Lett.* **38**, 1096–1104 (2011).
13. Erfanian, A., Wang, G. & Fomenko, L. Unprecedented drought over tropical South America in 2016: significantly under-predicted by tropical SST. *Sci. Rep.* **7**, 5811 (2017).
14. Hua, W. et al. Possible causes of the Central Equatorial African long-term drought. *Environ. Res. Lett.* **11**, 124002 (2016).
15. Hirota, M., Holmgren, M., Van Nes, E. H. & Scheffer, M. Global resilience of tropical forest and savanna to critical transitions. *Science* **334**, 232–235 (2011).
16. Schamm, K. et al. *GPCC Full Data Daily Version 1.0 at 1.0: Daily Land-surface Precipitation from Rain-gauges Built on GTS-based and Historic Data* (GPCC, 2015); https://doi.org/10.5676/DWD_GPCC/FD_D_V1_100
17. Xie, P. et al. GPCP pentad precipitation analyses: an experimental dataset based on gauge observations and satellite estimates. *J. Clim.* **16**, 2197–2214 (2003).
18. Xie, P. & Arkin, P. A. Global precipitation: a 17-year monthly analysis based on gauge observations, satellite estimates, and numerical model outputs. *Bull. Am. Meteorol. Soc.* **78**, 2539–2558 (1997).
19. Gelaro, R. et al. The modern-era retrospective analysis for research and applications, version 2 (MERRA-2). *J. Clim.* **30**, 5419–5454 (2017).
20. Pinzon, J. E. & Tucker, C. J. A non-stationary 1981–2012 AVHRR NDVI3g time series. *Remote Sens.* **6**, 6929–6960 (2014).
21. Liu, Y. Y., Dijk, A. I., McCabe, M. F., Evans, J. P. & Jeu, R. A. Global vegetation biomass change (1988–2008) and attribution to environmental and human drivers. *Glob. Ecol. Biogeogr.* **22**, 692–705 (2013).
22. Joiner, J. et al. Global monitoring of terrestrial chlorophyll fluorescence from moderate-spectral-resolution near-infrared satellite measurements: methodology, simulations, and application to GOME-2. *Atmos. Meas. Tech.* **6**, 2803–2823 (2013).
23. Masih, I., Maskey, S., Mussá, F. & Trambauer, P. A review of droughts on the African continent: a geospatial and long-term perspective. *Hydrol. Earth Syst. Sci.* **18**, 3635 (2014).
24. Ridolfi, L., D'Odorico, P. & Laio, F. Effect of vegetation–water table feedbacks on the stability and resilience of plant ecosystems. *Wat. Resour. Res.* **42**, W01201 (2006).
25. Dyer, E. L. et al. Congo Basin precipitation: assessing seasonality, regional interactions, and sources of moisture. *J. Geophys. Res. Atmos.* **122**, 6882–6898 (2017).
26. Berg, A. et al. Land-atmosphere feedbacks amplify aridity increase over land under global warming. *Nat. Clim. Chang.* **6**, 869–874 (2016).
27. Dargie, G. C. et al. Age, extent and carbon storage of the central Congo Basin peatland complex. *Nature* **542**, 86 (2017).
28. Potapov, P. et al. The last frontiers of wilderness: tracking loss of intact forest landscapes from 2000 to 2013. *Sci. Adv.* **3**, e1600821 (2017).
29. Baccini, A. et al. Tropical forests are a net carbon source based on aboveground measurements of gain and loss. *Science* **358**, 230–234 (2017).
30. Cox, P. M., Betts, R. A., Jones, C. D., Spall, S. A. & Totterdell, I. J. Acceleration of global warming due to carbon-cycle feedbacks in a coupled climate model. *Nature* **408**, 184–187 (2000).

Acknowledgements

This study is supported by National Science Foundation (NSF No. AGS-1535426). MERRA-2 reanalysis data were obtained from the Goddard Earth Sciences Data and Information Services Center. The ECMWF interim reanalysis data were obtained from the ECMWF data server.

Author contributions

Y.J. and L.Z. designed the research. All authors collectively analysed the data. Y.J. prepared the figures and wrote the first draft of this paper. L.Z., C.J.T., A.R., W.H., Y.Y.L. and J.J. contributed to refining the ideas and revising this paper.

Competing interests

The authors declare no competing interests.

Additional information

Supplementary information is available for this paper at https://doi.org/10.1038/s41558-019-0512-y.

Reprints and permissions information is available at www.nature.com/reprints.

Correspondence and requests for materials should be addressed to L.Z.

Peer review information: *Nature Climate Change* thanks Hans Verbeeck, Jessica Baker and other, anonymous, reviewer(s) for their contribution to the peer review of this work.

Publisher's note: Springer Nature remains neutral with regard to jurisdictional claims in published maps and institutional affiliations.

© The Author(s), under exclusive licence to Springer Nature Limited 2019

Methods

High-frequency precipitation datasets. Considering the low-gauge density over the Congo Basin (Supplementary Fig. 7)[31], this study adopted three widely used precipitation datasets that combine ground observations and satellite retrievals and one reanalysis dataset (Supplementary Table 1). To quantify the variations in the JJA dry season over central equatorial Africa from the hydrological perspective, we used the observational gridded daily rainfall data from the GPCC[16] at 1°×1° resolution (1988–2013), the pentad (5-d) data from the GPCP[17] at 2.5°×2.5° resolution (1979–2014) and the CPC CMAP[18] data at 2.5°×2.5° resolution (1980–2015). The daily GPCC data were produced based on abundant in situ observations and high-tech interpolation methods conducted by the World Meteorological Organization[16]. Both GPCP and CMAP precipitation have the advantage of combining gauge (including GPCC) and satellite observations. All three precipitation datasets were assessed using a newly created gauge-based monthly precipitation dataset[32] over central equatorial Africa (details available in Supplementary Information Section A). Another hourly reanalysis dataset from the National Aeronautics and Space Administration (NASA) MERRA-2 (ref. [19]), with land surface diagnostics at 0.625°×0.5° resolution for the period 1980–2015, was also utilized. MERRA-2 can reproduce the observed rainfall climatology, patterns and variability over central equatorial Africa more efficiently than other available reanalysis products[33,34]. Monthly reanalysis of root zone soil moisture data for the period 1980–2015 from CPC (at 0.5° resolution)[35], MERRA-2 (at 0.625°×0.5° resolution)[36] and ERA-Interim (at 1.0° resolution)[37] were used as auxiliary parameters to measure water availability.

Satellite-derived vegetation variables. Three satellite-derived vegetation datasets were analysed to quantify variations in the JJA DSL over the Congo Basin from the ecological perspective. We chose the widely used bi-weekly maximum value composite NDVI3g (ref. [20]) from the third-generation Global Inventory Modeling and Mapping Studies, generated based on Advanced Very High Resolution Radiometer data at 8-km resolution from 1982 to 2015. This dataset has been verified as having the best calibration and is the most accurate in terms of temporal changes in vegetation[38] (Supplementary Information Section C). Nevertheless, as calculated from the red and near-infrared solar reflectance, NDVI over tropical forests is probably impacted by clouds and atmospheric aerosols, which raise data uncertainties and noise in surface reflectance data[39]. Hence, empirical orthogonal functions were applied to decompose the NDVI data into various spatial and temporal components for the long-term, large-scale pattern analysis[40,41]. Combined with the cloud mask available within this dataset, the first six components explaining 77% of the original data variance were used to reconstruct the NDVI data. To validate the NDVI3g results, dry season changes (Supplementary Fig. 8) and available good-quality observations (Supplementary Figs. 9 and 10) were compared between NDVI3g and other Moderate Resolution Imaging Spectroradiometer vegetation products (Supplementary Information Section B). The DSL trend was further verified by other long-term NDVI records (Supplementary Fig. 11).

A newly merged daily VOD[21] at 0.25° spatial resolution, from 1993 to 2012, was derived from a series of passive microwave satellite sensors, including Special Sensor Microwave Imager, Advanced Microwave Scanning Radiometer, Fengyun-3B Microwave Radiometer Imager and Windsat. VOD measures the dynamics of water content within vegetation and is less sensitive to abundant clouds and atmospheric aerosols than the NDVI dataset. In addition, to make results comparable to precipitation, these two vegetation datasets were remapped on a 1.0° grid box using the nearest neighbour interpolation.

A newly developed dataset of solar-induced fluorescence (SIF v.27)[22,42], from 2007 to 2016, was also used from the Global Ozone Monitoring Experiment instrument on the MetOp-A satellite. SIF is emitted from chlorophyll during photosynthesis and is primarily driven by the amount of absorbed photosynthetic radiation[43]. Although chlorophyll fluorescence has been used as a major tool for basic research in photosynthesis for many years[44], it was discovered recently that SIF can be retrieved from space using moderate spectral resolution radiances and has provided a new proxy for global plant photosynthesis[43]. Here, the 40×80 km^2 individual SIF observations were processed into 5-d time steps at a spatial resolution of 2.5°.

Definition of dry season onset and end. The variety of rainfall regimes over Central Africa complicates the characterization of the seasonality. Rather than setting a unified precipitation threshold, such as 100 mm d^{-1} as done in previous studies, the method based on calculation of cumulative rainfall anomaly[45,46] was adjusted and applied to identify the onset and end of the dry season. First, the climatological pentad (5-d) mean rainfall rate $\overline{P}$ was calculated using the data from all months in all years, and from this the annual cumulative pentad rainfall anomaly on pentad d, $A(d)$ was found:

$$A(d) = \sum_{j_0}^{d} (P_j - \overline{P}) \quad (1)$$

where P_j is the rainfall on pentad j and j ranges from March (j_0) to the pentad d being considered. $A(d)$ was calculated from March to November to include the JJA dry season. $A(d)$ increases when the pentad precipitation is above the climatological mean and decrease when the precipitation is below the climatological mean 5-d rainfall (Supplementary Fig. 3). Thus, the day of maximum $A(d)$ is the DSO and the day of minimum $A(d)$ is the DSE. This method was applied to all datasets mentioned above to explore the spatial pattern of climatology and trends of the dry season.

Long-term trend analysis. Before the trend analysis, all precipitation and vegetation datasets were interpolated onto the unified pentad temporal resolution. After identifying the DSE and DSO, annual DSL in days can be calculated as the difference between DSE and DSO within each grid box over the study region. Two methods were used to quantify and validate the temporal changes at both the grid and regional level. First, the linear trend of annual DSL time series was estimated using ordinary least squares regression over the same time period for each grid box. Its statistical significance level (P) was assessed by the two-tailed Student's t-test to verify whether the trend was statistically significant rather than random noise. Trends of DSO and DSE were estimated similarly. Second, the non-parametric Mann–Kendall trend test was applied on the time series of DSL, DSO and DSE to detect whether a significant monotonic increasing or decreasing trend exists. The P value was also measured by the two-tailed Student's t-test. The Mann–Kendall test provides additional verification for the robustness of the linear regression trend analysis, as it is less sensitive to the beginning and end of the analysis period. In particular, for the spatial pattern of DSL trends, results were plotted only for grids with annual rainfall >250 mm and a dry spell of at least 5 d, to avoid singular and inauthentic trends over extreme dry or wet grids[47]. Similarly, trends were shown only for grids with annual mean NDVI > 0.3 (refs. [5,20]), VOD > 0.4 (ref. [21]), SIF > 0.4 (ref. [48]) and a dry spell of at least 5 d for satellite-derived vegetation variables. Finally, to maximize large-scale features while minimizing local-scale variability and noise, the time series of DSL/DSO/DSE at the regional aggregated level were calculated using area-weighted averaging over the Congo Basin (12° E–32° E, 5° N–6° S). The corresponding linear trends of DSL/DSO/DSE at the regional level were estimated as done at the grid level.

Data uncertainties. Due to insufficient observations over the Congo Basin, we used reanalysis and satellite datasets to study the variations in precipitation and vegetation seasonality. Our analyses indicate a comparable and consistent increasing trend in the JJA DSL from all datasets for the period 1979–2015 and similar peaks of DSL around 2004 and 2005 at the regional level. However, there are some discrepancies in the magnitude and spatial distribution of DSL trends that may have resulted from data uncertainties and the different approaches used to generate homogeneous climate records.

For the precipitation datasets, gauge-based GPCC and satellite-combined CMAP and GPCP are quite sensitive to the number and density of observations used[16–18]. Due to sparse observational stations over the Congo Basin, different interpolation methods were adopted to fill data gaps, which might have generated errors in the rainfall products. For satellite-retrieved vegetation variables, effects of satellite change-over, orbital drifts, volcanic aerosols and changes in solar zenith angle have been corrected, but residual non-vegetation signal may still remain. Despite intensive cloud screening and preprocessing, NDVI may still contain residual non-vegetation signals due to contamination of sub-pixel clouds and biomass burning, which can cause spurious NDVI changes (Supplementary Information Section B)[49]. In addition, bi-weekly temporal resolution may miss the detailed temporal evolution of NDVI phenology on time scales shorter than two weeks. VOD is less affected by clouds and aerosols because it measures water content contained in biomass via passive microwave radiation. Nevertheless, VOD is underestimated when there are substantial open water bodies in the observation footprint[21,50]. The SIF dataset includes noise due to instrument degradation[42]. Overall, these issues probably introduced some uncertainties in our estimates of dry season changes.

Data availability

The daily and monthly GPCC precipitation datasets are available at https://doi.org/10.5676/DWD_GPCC/FD_D_V1_100. The 5-d GPCP precipitation data are available at https://precip.gsfc.nasa.gov/. The 5-d CMAP precipitation data are available at https://www.esrl.noaa.gov/psd/data/gridded/data.cmap.html. The satellite-observed NDVI datasets are available from the NASA Earth Exchange (NEX) website (https://nex.nasa.gov/nex). VOD and SIF datasets are available upon request from L.Z.

Code availability

The Python language was used to generate all results. Scripts are available upon request from L.Z.

References

31. Washington, R., James, R., Pearce, H., Pokam, W. M. & Moufouma-Okia, W. Congo Basin rainfall climatology: can we believe the climate models? *Philos. Trans. R. Soc. Lond. B* **368**, 20120296 (2013).

32. Nicholson, S., Klotter, D., Dezfuli, A. & Zhou, L. New rainfall datasets for the Congo Basin and surrounding regions. *J. Hydrometeorol.* **19**, 1379–1396 (2018).
33. Molod, A., Takacs, L., Suarez, M. & Bacmeister, J. Development of the GEOS-5 atmospheric general circulation model: evolution from MERRA to MERRA2. *Geosci. Model Dev.* **8**, 1339–1356 (2015).
34. Hua, W., Zhou, L., Nicholson, S. E., Chen, H. & Qin, M. Assessing reanalysis data for understanding rainfall climatology and variability over Central Equatorial Africa. *Clim. Dynam*. https://doi.org/10.1007/s00382-018-04604-0 (2019).
35. Fan, Y. & van den Dool, H. Climate Prediction Center global monthly soil moisture data set at 0.5 resolution for 1948 to present. *J. Geophys. Res. Atmos.* **109**, D10102 (2004).
36. Reichle, R. H. et al. Assessment of MERRA-2 land surface hydrology estimates. *J. Clim.* **30**, 2937–2960 (2017).
37. Albergel, C., De Rosnay, P., Balsamo, G., Isaksen, L. & Muñoz-Sabater, J. Soil moisture analyses at ECMWF: evaluation using global ground-based in situ observations. *J. Hydrometeorol.* **13**, 1442–1460 (2012).
38. Beck, H. E. et al. Global evaluation of four AVHRR–NDVI data sets: intercomparison and assessment against Landsat imagery. *Remote Sens. Environ.* **115**, 2547–2563 (2011).
39. Asefi-Najafabady, S. & Saatchi, S. Response of African humid tropical forests to recent rainfall anomalies. *Philos. Trans. R. Soc. Lond. B* **368**, 20120306 (2013).
40. Eastman, J. R. & Filk, M. Long sequence time series evaluation using standardized principal components. *Photo. Eng. Remote Sens.* **59**, 991–996 (1993).
41. Anyamba, A. & Tucker, C. J. in *Remote Sensing of Drought: Innovative Monitoring Approaches* (eds Wardlow B. D. et al.) Ch. 2 (CGR Press, 2012).
42. Joiner, J., Yoshida, Y., Guanter, L. & Middleton, E. M. New methods for the retrieval of chlorophyll red fluorescence from hyperspectral satellite instruments: simulations and application to GOME-2 and SCIAMACHY. *Atmos. Meas. Tech.* **9**, 3939–3967 (2016).
43. Sun, Y. et al. Overview of solar-induced chlorophyll fluorescence (SIF) from the orbiting carbon observatory-2: retrieval, cross-mission comparison, and global monitoring for GPP. *Remote Sens. Environ.* **209**, 808–823 (2018).
44. Krause, G. & Weis, E. Chlorophyll fluorescence and photosynthesis: the basics. *Annu. Rev. Plant Physiol. Plant Mol. Biol.* **42**, 313–349 (1991).
45. Liebmann, B. et al. Seasonality of African precipitation from 1996 to 2009. *J. Clim.* **25**, 4304–4322 (2012).
46. Dunning, C. M., Black, E. C. & Allan, R. P. The onset and cessation of seasonal rainfall over Africa. *J. Geophys. Res. Atmos.* **121**, 405–24 (2016).
47. Yang, W., Seager, R., Cane, M. A. & Lyon, B. The annual cycle of East African precipitation. *J. Clim.* **28**, 2385–2404 (2015).
48. Joiner, J., Yoshida, Y., Vasilkov, A. & Middleton, E. First observations of global and seasonal terrestrial chlorophyll fluorescence from space. *Biogeosciences* **8**, 637–651 (2011).
49. Tucker, C. J. et al. An extended AVHRR 8-km NDVI dataset compatible with MODIS and SPOT vegetation NDVI data. *Int. J. Remote Sens.* **26**, 4485–4498 (2005).
50. Liu, Y. Y. et al. Recent reversal in loss of global terrestrial biomass. *Nat. Clim. Chang.* **5**, 470 (2015).